International Journal of Innovative Research and Reviews, 6(1) 18-25

International Journal of Innovative Research and Reviews
ISSN: 2636-8919
Website: www.injirr.com
doi:
Research paper, Short communication, Review, Technical paper

RESEARCH ARTICLE

The Effect of Adding La_2O_3 and Fe_2O_3 Binder to the Thick Film SnO_2 Sensor on the Sensor's Properties

Elif AKARSU[1,*] Demet İSKENDEROĞLU[2] Mehmet ERTUĞRUL[1]

[1] *Department of Electrical-Electronics Engineering, Faculty of Engineering, Ataturk University, Erzurum, Turkiye*
[2] *Department of Science Education, Faculty of Education, Ataturk University, Erzurum, Turkiye*

** Corresponding author E-mail: elif.akarsu@atauni.edu.tr*

HIGHLIGHTS

> It has been observed that the La_2O_3 contribution to SnO_2 shortens the sensor response time and increases the sensor operating performance.
> The negative effects of the Fe2O3 additive on the thick film sensor were observed.

ARTICLE INFO

Received : 12.21.2021
Accepted : 04.18.2022
Published : 07.15.2022

Keywords:
Thick film,
Gas sensor
Metal oxide
Screen printing
Paste
Binder

ABSTRACT

In this study, the features of the SnO2 gas sensor were examined and the effects of metal oxide semiconducting requisites such as La2O3 and Fe2O3 on the gas sensor system were searched. Sensor fabrications were carried out with thick film sensor design. In order to obtain these thick film sensors, a mixture called binder was transferred from nano-sized masks to alumina surfaces by screen printing technique. The name of this mixture is binder. Binder mixture consists of ethyl cellulose, alpha terpineol, active powder mixture. However, in order to obtain a quality sensor, it is necessary to pay attention to the proportion of this mixture, the mixing times and temperatures. A binder was prepared by adding 30% active powder to the paste solution taken in the ratio of 70% by weight. Ethyl cellulose was mixed with alpha terpineol at 40 °C for 3 hours at 150 rpm at 1:10.

Contents

1. Introduction

In this study, SnO_2 metal oxide semiconductor gas sensors containing SnO_2, La_2O_3, and Fe_2O_3 were obtained by a screen-printing technique, and the effect of $La_2O_3$and Fe_2O_3 additive on structural and morphological properties was investigated. Nanostructured materials are an excellent candidate for ultrasensitive and solid-state gas sensors due to their high surface/volume ratio and special Physico-chemical

Cite this article Akarsu E, İskenderoğlu D, Ertuğrul M. The Effect of Adding La_2O_3 and Fe_2O_3 Binder to The Thick Film SnO_2 Sensor on The Sensor's Properties. *International Journal of Innovative Research and Reviews (INJIRR)* (2022) 6(1) 18-25
Link to this article: http://www.injirr.com/article/view/92

properties. Tin oxide (SnO_2) is a well-known n-type semiconductor with wideband energy of 3.62 eV and has been adopted for its electrochemical properties suitable for gas sensor applications. SnO_2-based gas sensors have been the subject of many studies due to their relatively low operating temperatures, long-term stability, and low-cost advantages. Small size of SnO_2 particles plays an important role for mentioned applications. The size of tin oxide particles can be controlled by small number of additives such as metal oxides and noble metals.

Semiconductor based oxide material was used over many years as sensing materials for fabrication of gas sensors. The concentration of charges, which are brought on the surface of semiconductor gas sensors, is sensitive to the composition of surrounding atmosphere. Therefore, these materials were employed for detection of different gases [1, 2]. SnO_2 is one of the most important metal oxide materials, which is used as the base material for fabrication of gas sensors [3, 4]. The sensors included in this study were obtained by simple and economical screen-printing method which does not require any technological device and infrastructure [5]. Thick film technology is one part of the microelectronic process technology for fabricating electronic components using the screen-printing method. Since the mid1960s, because of its ability to produce very small conductor lines (fine lines), thick film technology has been used to miniaturize an electronic circuit into a substrate chip [6]. The technology that uses thick film can produce multiple layers on one or both sides of the bottom layer. It has many advantages such as low expenditure, high precision, chemical, and mechanical determination. For this reason, low-cost SnO_2, La_2O_3 doped SnO_2, and Fe_2O_3 doped SnO_2 metal oxide gas sensors with good sensing properties in the gas environment were obtained using this technology, and structural, morphological, and sensor properties were investigated [5].

Screen printing is a thick film enlargement technique. Masks are used in the required shapes for the manufacture of the gas sensor. There are different areas for different applications on the mask (organic solar cell, electrodes for resistance measurements in gas sensor applications, and active layer section, etc.). It is a production technique that has a very low cost compared to other methods. It requires less equipment than other amplification techniques, so it is one of the most suitable methods for use in research studies. Also, the production volume can be increased with industrial-type screen printing devices in this production technique. The production of sensing layers by screen-printing technology has met the interest of the scientists working in the field. In fact, screen-printing is a simple and automated manufacturing technique that allows the production of low-cost and robust chemical sensors with good reproducibility [7]. Because there is no system requirement for fabrication. This technique allows a controlled amount of paste to be deposited at a thickness ranging from a few nanometers to a few micrometers. This paste is used in screen printing. One of the pastes is obtained for high temperatures and one for low temperatures. Organics in the cakes should evaporate during tempering. This evaporation takes place at very high temperatures. If the organic substances in the paste do not evaporate sufficiently, the sensor response cannot be obtained. Another point to be considered about pastes is the prevention of oxygen and carbon accumulation in the environment on the metal oxide semiconductor. To prevent this, the sensors must be annealed in a nitrogen environment. Besides, the compatibility of the paste and substrate used in the production process is an important parameter. Alumina mats are often used for screen printing. There are two reasons for this. First, the rough surface of alumina increases the fixation amount of the active powder, and the other is that the alumina is resistant to high annealing temperature. Screens are used in the serigraphy technique. The screen is made of finely woven fabric. This fabric is made of silk by creating nano-sized openings. The organic compound we get must pass through these gaps. Organic material passing through these gaps accumulates on the substrate. The concentration of charges, which are brought on the surface of semiconductor gas sensors, is sensitive to the composition of surrounding atmosphere [8].

Therefore, these materials have been used to detect different gases. Semiconducting metal oxide-based gas sensors have a small dimensions, low cost, fast response, and recovery time [9]. Different sensing technologies have been employed to detect hydrogen, such as catalyst, thermal conductivity, electrochemical, resistance based, work function based, mechanical, and optical [10].

The catalytic properties of rare earth metal oxides such as La_2O_3 can be activated by the acidic site of tin oxide. Moreover, the electronic distribution of materials is affected by rare earth chain of this material which acts as adsorbing center. La_2O_3 is one kind of rare earth metal oxides hexagonal and cubic crystalline structure at low and high temperature respectively. Adsorption of a gas on the surface of a metal oxide semiconductor material can bring about a significant change in the electrical resistance of the material. During the conversion, a number of physical and chemical parameters such as film thickness, grain size, intergrain contact, porosity, grain network, phase composition, elemental composition, bulk stoichiometry, surface architecture, type of additives and dopants, etc. are involved in the changes of conductance of the oxide when the film is exposed to a gaseous atmosphere [11].

2. Materials and Method

The active printing (active layer) stage was realized. There are masks required for this process. Two important parameters of the screen-printing fabric used in the screen-printing method are the "w", the gap between the yarns, and the "d", the diameter of the wire. These parameters are shown in Figure 1.

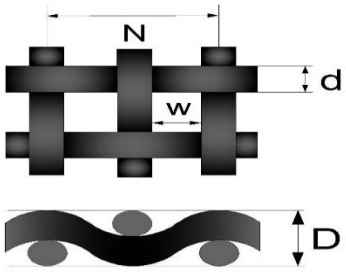

Figure 1 Schematic structure of the screen fabric

The "N" is called the number of threads per unit length and indicates the fineness of the screen. Shows the open area ratio of the screen outdoors. A high open area ratio means that the solution or paint passes further from the screen to the print surface. The theoretical amount of binding to the maximum amount of ink that can pass through the screen on the print screen is called "Vth". Vth is for working with printing dye or solution screen, the screen display of various screen images of screen fabric, and the open area ratio of this screen and screen area "D" caused by other cable usage and weaving techniques. The Vth unit can be determined by the type of fabric in the thick film thickness that will result from the printing.

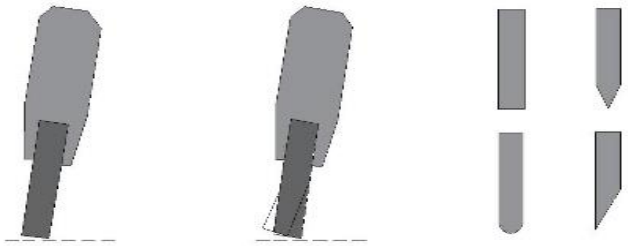

Figure 2 Side view of a wiper

Some of the organic ingredients called cakes are glued to these masks and pulled with the help of a rubber cuff. This arm is called a wiper blade. Wiper blades made from different materials are usually made of polymer and rubber. The hardness and the correct angle of this tire, as well as the tip profile, affect the quality of the process (Figure 2).

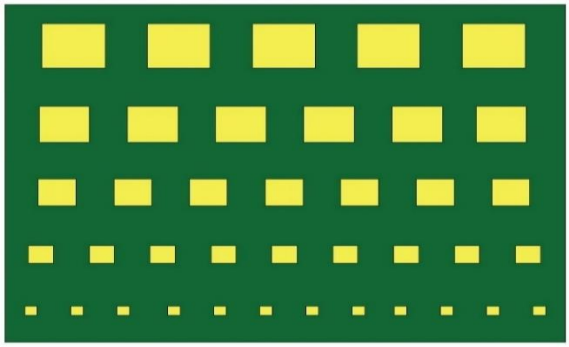

Figure 3 Special mask of the active layer

Figure 3 shows the different wiper sections. Besides, wiper blade wear is an important parameter. On these masks, some organic ingredient called pastry is placed with the help of a rubber arm. This arm is called a wiper blade. Wiper blades made from different materials are usually made of polymer and rubber.

2.1. Basic screen printing

For the production of thick film using the screen-printing technique, the process starts by fixing the sieve and the distance between the bottom and the curtain should be placed. The reason we do this is to allow the cake to accumulate homogeneously on the surface and to prevent the alumina surface from sticking to each other. After a sufficient amount of organic paste is placed on the screen, it is drawn in one direction with a squeegee. With the print of the squeegee rubber, the organic paste is deposited on the lower stone through the openings on the screen. This process is shown schematically in Figure 4.

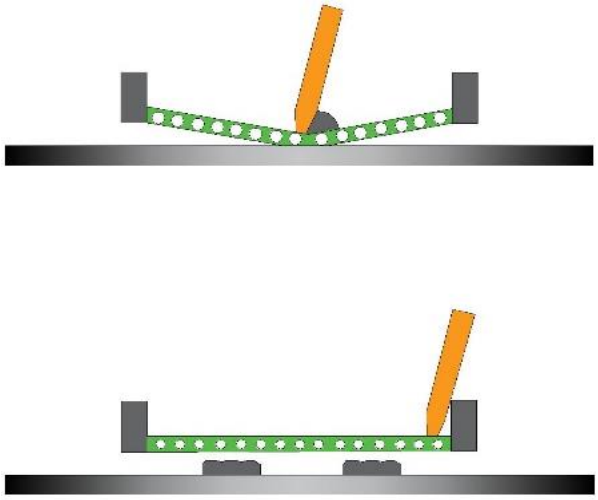

Figure 4 Top and side view of the system

2.2. Annealing in a nitrogen environment

Crystals are annealed to get a more regular, lower energy structure. Annealing is the process of heating the crystal to a temperature close to its melting temperature, then cooling it slowly and waiting for a while considering the properties of the material. The waiting period can last from 15 minutes to several days, in line with the goals set in the study. In this study, annealing was carried out at 650 ° C for 30 minutes under nitrogen. The reason for annealing in a nitrogen environment is the minimum oxygen level accumulated in the structure.

2.3. Putty preparation with ethyl cellulose and alpha-terpineol

Ethyl cellulose was mixed with alpha-terpineol at 40 °C for 3 hours at 150 rpm at 1:10. The active powder addition is the same as for linseed oil. In this study, a paste was prepared by adding 30% active powder to the paste solution taken in the ratio of 70% by weight. But the amount varies by weight for different substances such as platinum or zinc. One of the important points here is that the active powder must be ground and sieved before being added to obtain the material of the desired grain size. The prepared dough is mixed by hand until the beaker is stable (to prevent slipping). Thus, the cake formed becomes ready to use. Finally, it was dried at 150 ° C for 10 minutes. It was then heat-treated at 700 ° C for 30 minutes.

2.4. Ohmic contact process

The ohmic contact manufacturing made by thermal evaporation is made with four heat sources, respectively, and is metalized with Ag metal by evaporating from two crucibles together. With the rotating hot sample holder, contacts of equal thickness are prepared. In this study, ohmic contact at 30 nm thickness was made on the samples prepared by a screen-printing method using silver metal. The silver metal was evaporated at a pressure of 1 x 10^{-7} Torr for 3-4 minutes.

3. Characterization

3.1. XRD characterization

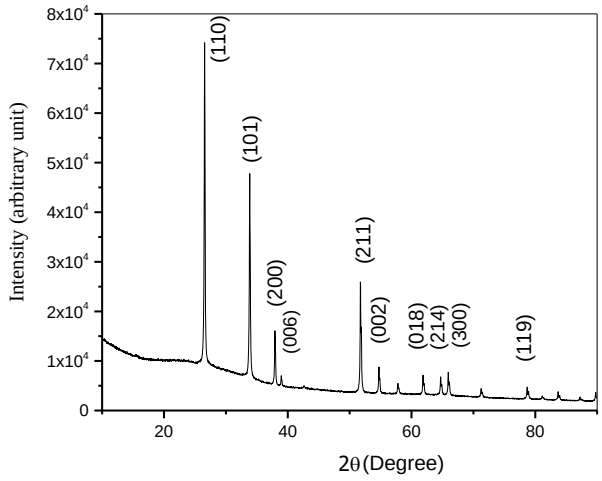

Figure 5 Reflection planes of SnO_2

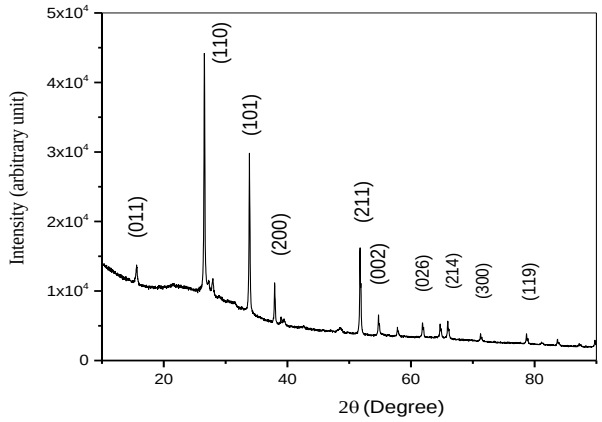

Figure 6 Reflection planes of La_2O_3 doped SnO_2

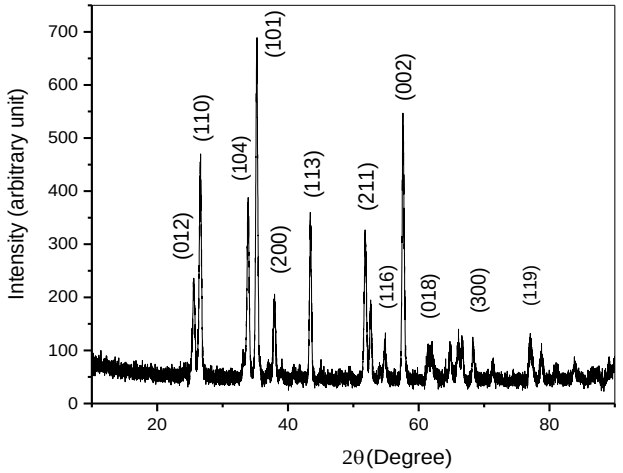

Figure 7 Reflection planes of Fe_2O_3 doped SnO_2

It can be seen in Figure 5 that the SnO_2 contribution is reflected on the planes (110), (101), (211), (200), and (002). When these reflecting planes are compared with other studies, it is seen that pure SnO_2 has reflective peaks. Besides, reflected peaks from the substrates of the Al_2O_3 substone material (018), (300), (006), and (214), (119) were detected. When the obtained XRD results were examined, it was seen that the density of the peaks was strong. This is because the size of the nanoscale active powder used is suitable for sensor fabrication and crystallization is high as a result of annealing at about 700 ° C showed that particle size decreased. It can be said that the reduction in particle size depends both on the size of the active powder used and the amount of deposition on the substrate.

The XRD result given in Figure 6 belongs to $SnO_2$with La_2O_3. The reflection planes of SnO_2 (110), (101), (211), (200) and (002) were observed. Since La_2O_3 was added to the structure, the peaks of (011) and (026) of La_2O_3 and (214), (300), (119) were determined, reflecting the La_2O_3 planes, which are the substrate material FWHM (full width at half maximum) is a two-dimensional wide-ranging, spherical wide-ranging two-point wide-range. The peak intensity of the sensor decreased to pure SnO_2 and as a result, the FWHM (full width at half maximum) value increased. This caused particle size reduction and crystallization and increased sensor detection area. In the study, it was observed that the peak densities were stronger and the particle size decreased and crystallization was better compared to the study with La_2O_3 added to SnO_2.

The Fe_2O_3 doped XRD analysis of SnO_2 is given in the Figure 7. (110), (101), (211), (200), and (002) SnO_2 peaks were observed. Fe_2O_3, which reflects the planes (116) and (012), (119), (300), (018) (116) and (012), (119), (300), (018), as Fe_2O_3 is added to the structure. It was determined that the peak density of the sensor decreased compared to pure SnO_2. Particle size increased and crystallization deteriorated. Compared the study by the addition of Fe_2O_3 to SnO_2. similar to our results, it was observed that peak densities were lower, particle size increased, and crystallization was worse.

Table 1 Lattice parameters and particle size

	d(Å)	a(Å)	c(Å)	D(nm)
SnO_2	2,36	4,72	3,34	37,24
%10 La_2O_3+ SnO_2	2,36	4,72	3,34	32,02
%10 Fe_2O_3+ SnO_2	2,36	4,736	3,35	42.94

The values of the distance between planes (**d**) are determined by Bragg's law.

$$n * \lambda = 2 * d * sin\theta \quad (1)$$

In equation (1), n is equal to 1, λ, and θ is respectively the wavelength and diffraction angle of the X-ray beam.

The lattice constants are calculated by:

$$\frac{1}{d^2} = 4/3\ (\frac{(h^2 + k^2 + h * k)}{a^2}) + (\frac{l^2}{c^2}) \quad (2)$$

where d is the interplanar separation h, k, l are the crystal plane index, **a**, and **c** are lattice parameters respectively. The calculated values of "a" and "c" matched well with reported. [12]

(a = 4,72Å, c = 3,34Å).

The crystal quality of SnO_2 thick films is determined according to the crystallite size calculated from the peak measurements in the diffraction pattern. The crystallite size (D) in the film was determined using Scherrer's formula [13].

$$D = 0.9 * \lambda/\beta * cos\theta \quad (3)$$

Where β is full width at half maximum (FWHM) and it is determined using Eq [12].

$$\beta^2 = \beta_{obs}^2 - \beta_{Inst}^2 \quad (4)$$

Inst. B_{obs} and β_{inst} are the values in XRD peak and instrumental broadening [12].

3.2. SEM characterization

SEM is a type of electron microscope that obtains an image by scanning the sample surface with a focused beam of electrons. Electrons interact with atoms in the sample, producing different signals that contain information about the topography and composition on the sample surface. In SEM, the secondary electrons emitted by the sample atoms excited by the electron beam are mostly used to form the image. Secondary electrons are produced from collisions of weakly bound electrons in the outer orbitals of the atom. They are low energy electrons. The change in the number of secondary electrons ejected from different parts of the sample primarily depends on the meeting angle of the electron beam with the surface, that is, on the topography of the surface.

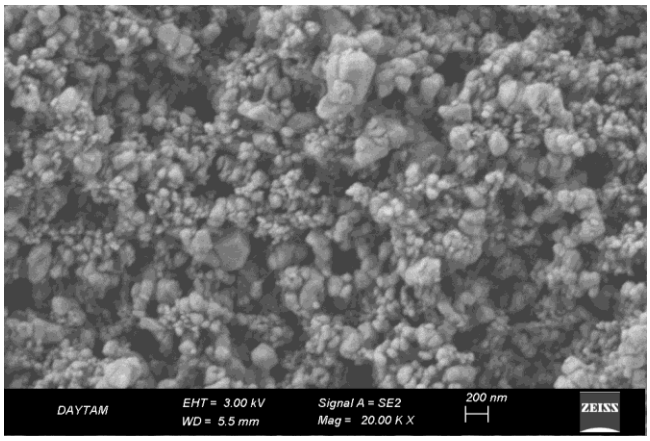

Figure 8 SEM images of SnO_2 thick film

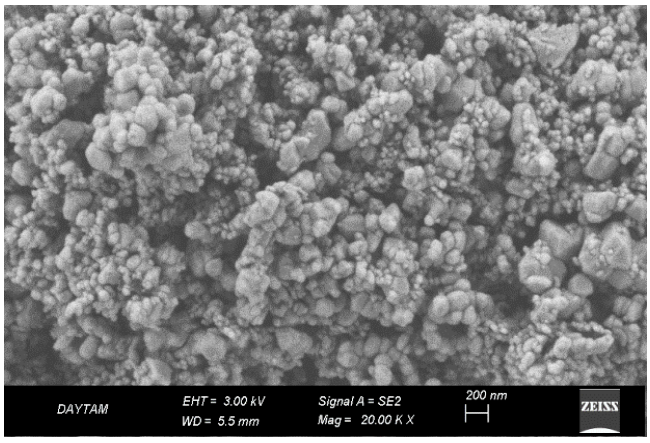

Figure 9 SEM images of La_2O_3 doped SnO_2 thick film

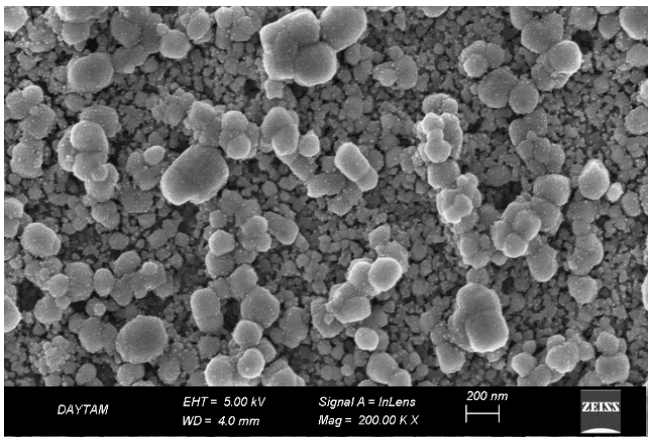

Figure 10 SEM images of Fe_2O_3 doped SnO_2 thick film

The samples examined in SEM do not have to be conductive. All kinds of metals and plastics can be examined. Non-conductive samples are covered with a very thin (approximately 3 Å) conductive material and made to be examined. Non-liquid and non-liquid samples are examined in a high vacuum scanning electron microscope.

The different resolution SEM images given in the Figure 8 are of SnO_2 thick film annealed at 700 °C for 30 minutes. From the SEM images, it was determined that the particles spread in a homogeneous pattern, but there were size differences between the particle sizes and the porous structure of the surface. This porous structure has shown very high performance in holding gas.

In Figure 9, different resolution SEM images are given in the figure. It belongs to thick film with 10% La_2O_3 added into SnO_2 annealed for 30 minutes at 700 ° C. As the structure is strengthened, hexagonal structures are encountered. These hexagonal structures have increased the gas's ability to adhere to the surface. There are also large voids between the particles, i.e. the surface topography is porous. This potential significantly affects the response of the sensor. Compared to pure SnO_2, it was observed that the small particle size supporting XRD analysis was reduced.

In Figure 10, SEM images of 10% Fe_2O_3 doped thick film are added to SnO_2 annealed at 700 ° C for 30 minutes at different resolutions. It has been observed that the accumulation of metal oxide semiconductor particles is as stable and porous as possible. However, as it is structure-doped, there are also large-sized particles compared to pure SnO_2. These large particles greatly reduced the sensor's surface area in gas detection and increased sensor response time. This harmed the sensor. These results supported the result in the XRD analysis.

Thick analysis and characterization of nanostructured SnO_2 in construction. The micron-diameter SnO_2 powder was then ground to fabricate the active powder in SnO_2 nano, which was grown by XRD and SEM. This powder was used as a thick film of tin oxide applied part. Scanning electron microscopy (SEM small and uniform particle) has been completed. The samples were exhibited with the small temperature required for the electrochemical structure. Plans for future work are included in the questionnaire [14]. Study, 40:60% and 60:40% by weight mixtures of Fe_2O_3 and TiO_2 were mixed with the paste. The sample was annealed at 800-850°C. XRD analysis are samples examined at monoclinic

800°C. Annealed at 850°C. Measurements of samples of samples of C6T and 6F4T samples, 6F4T samples, also had the potential for better analysis of gas sensors [15]. The first step of zeolite formulation with a mixture of Chromium Titanate to detect use gas in construction. It was observed that the gas sensor containing doped CTO metal oxide and 30% zeolite was observed with its targets for all gases at 350°C, 300°C and 250°C [16]. Many conductivity and capacitance measurements were made in thick-film devices that printed pure SnO_2 and catalyst samples. In the experimental results obtained, it was observed that the catalysts used had a great effect on the sensor performance [7]. Metal oxides added to SnO_2, annealing temperature of sensors and response characteristics of thick-film gas sensors were investigated. It has been observed that the optimum temperature for sensor operation is 600°C and WO_3 reduces the response time of the sensor [17]. Investigated the properties of the SnO_2 -based gas sensor and found that the power consumption was as low as 30 Mw at 400°C. In addition, the sensitivity of the sensor to nitrogen gas was investigated. As a result of the research, it has been determined that the catalysts used increase the sensitivity to gas [18].

4. Results and Discussion

The graph in the Figure 11 shows the measurement of pure SnO_2 gas sensors at 1000 ppm in 100 seconds and 600 seconds. The voltage of the source is 5 V. Its measurement temperature is 200 ° C. Firstly; nitrogen gas was sent to the environment in order to clean the environment from various gases. Then, the nitrogen gas was closed and the hydrogen gas to be measured was given to the environment. Hydrogen gas reacts with the remaining oxygen in the environment. The reaction equation is as follows.

$$2H_2+O_2 \longrightarrow 2H_2O+e^-$$

As a result of this reaction, a free electron is formed in the structure. Since tin oxide is an n-type metal oxide semiconductor, conductivity increases when the free electron in the structure increases. The conductivity increases when the hydrogen gas is in the environment and decreases suddenly when the gas is cut off. While this decrease was expected to be abrupt, this period was somewhat delayed. This is because the metal oxide semiconductor is an n-type material.

When the gas sensor graph of La_2O_3 doped SnO_2 in Figure 12 was examined, it was first seen that nitrogen gas entered the environment. This is because nitrogen sweeps the oxidized air from the environment. The hydrogen gas to be detected later was sent to the sensor. It was observed that the sensor response accelerated in the doped structure. In other words, when the hydrogen gas was cut off, the sensor became stable in no time. The reason is that La_2O_3 p-type metal oxide is a semiconductor. That is, it increases the number of voids in the structure while decreasing the number of free electrons. The increased void number decreased the repulsion force of electrons, causing a reduction in particle size. The reduced particle size increased the surface area of the gas sensor, thus speeding up the system response.

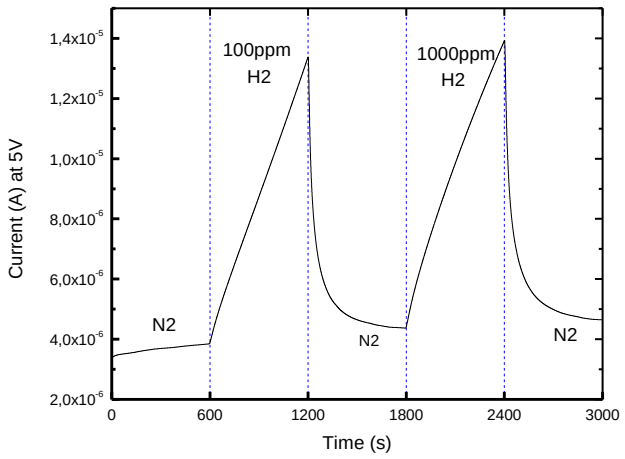

Figure 11 Gas sensor measurement chart of SnO_2

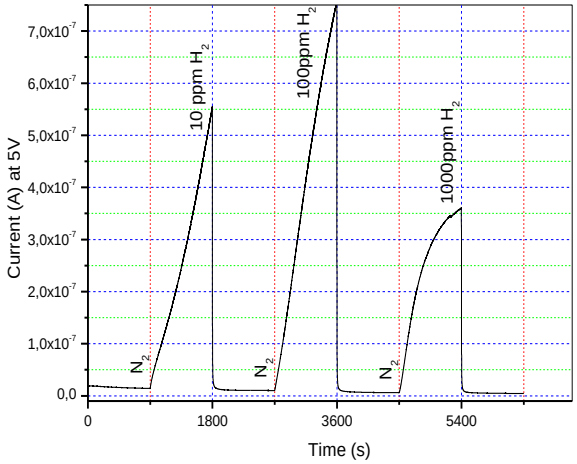

Figure 12 Gas sensor measurement graph of La_2O_3 doped SnO_2

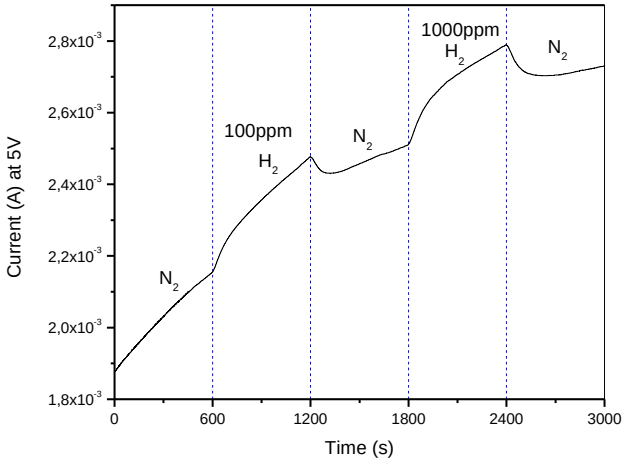

Figure 13 Gas sensor measurement chart of Fe_2O_3 doped SnO_2

When the gas sensor graphic of Fe_2O_3 doped SnO_2, given Figure 13, was examined, it was first observed that nitrogen gas entered the environment. This is because nitrogen sweeps the oxidized air from the environment. The hydrogen gas to be detected later was sent to the sensor. It was observed that the sensor response slowed down and deteriorated in the doped structure. In other words, when hydrogen gas is cut off, the sensor's stabilization is delayed. The reason is that Fe_2O_3 is an n-type metal oxide

semiconductor. That is, while increasing the number of free electrons, it decreases the number of holes in the structure. The decreasing hole number increased the repulsion force of the electrons, causing the particle size to increase. The increased particle size decreased the surface area of the gas sensor, causing the system to slow its response.

The response of the sensor to CO_2 gas at 225°C was measured. In the measurement graph obtained, it was observed that the response of the sensor accelerated as the gas density increased. However, in our study, the sensitivity of the same sensor to H_2 gas was measured at 200°C. According to the result obtained, it was observed that the response time of the sensor was faster against hydrogen gas. 10% Fe_2O_3 doped SnO_2 metal oxide semiconductor at 100,1000 ppm in 600 seconds and at 200°C is given [8]. The voltage of the source is 5V. By adding Fe_2O_3 to TiO_2, it was observed that the sensors were annealed at approximately 950°C. However, in this study, samples with Fe_2O_3 doped to SnO_2 were annealed at approximately 700°C. SnO_2 was found to have a positive effect on the sensor response. The reason is that the sensor response is accelerated despite the smaller annealing temperature. In this, crystallization, particle size and metal oxide material used have a significant effect [15].

5. Conclusion

The effects of metal oxide semiconductor materials such as La_2O_3, Fe_2O_3 on the gas sensor system were investigated. According to the XRD results obtained, it was observed that La_2O_3 doped SnO_2 had a decreasing particle size compared to undoped SnO_2, while Fe_2O_3 doped SnO_2 had an increasing particle size. In other words, it was determined that the intensity of the peaks obtained in the XRD results of the La_2O_3 doped semiconductor decreased compared to the pure SnO_2, therefore full width at half maximum value increased, which reduced the particle size. In the XRD results of the Fe_2O_3 doped semiconductor, it was observed that the peak intensities increased, the full width at half maximum value decreased, thus the particle size increased. Peaks from the alumina substrate used were observed. In the XRD results obtained, it was observed that the La_2O_3 additive improved the crystal structure of SnO_2, while the Fe_2O_3 additive had a negative effect on the crystallization.

In the SEM images taken, results compatible with the XRD data were obtained and the surface topography was examined. A homogeneous distribution was observed in pure SnO_2, and the indented structure of the surface was also detected. This indented structure has increased the gas holding capacity of the system and the effects of doping on this capacity have been investigated. It was observed that the particle sizes in the morphology of La_2O_3 doped SnO_2 decreased compared to pure SnO_2 and that hexagonal structures were formed and they were also in a homogeneous distribution. The large surface areas of the hexagonal structures obtained increased the adhesion capacity of the gas to the surface. And the small size particles have expanded the detection area of the gas. When SEM images of Fe_2O_3 doped SnO_2 were examined, large grains of Fe_2O_3were observed. These particles are homogeneously distributed on the surface. These large particles significantly reduced the adhesion capacity of the sensor gas to the surface. In addition, it was determined that the surface porosity decreased compared to pure SnO_2. The gas sensor responses of the obtained metal oxide semiconductor materials were investigated. Since La_2O_3 is a p-type metal oxide semiconductor, it increased the number of holes in the structure and caused a decrease in the number of electrons. In other words, the repulsive force created by the electrons decreased. This reduced the particle size of the gas sensor and increased the surface area used for gas detection. This increased surface area has increased the detection capacity of the gas sensor and shortened the response time. However, since Fe_2O_3 is an n-type semiconductor, it increased the number of electrons in the structure and caused the repulsion force, causing the particle size of the gas sensor to increase. This increased particle size reduced the sensing area of the sensor, greatly reducing the operating performance of the sensor.

In summary, in this study, we produced SnO_2, La_2O_3 doped SnO_2 and Fe_2O_3 doped SnO_2 semiconductor materials with the simple and economical screen-printing method and their structural and morphological properties were investigated. The gas sensor properties of the obtained materials were examined and a highly efficient sensor was obtained from tin oxide. In addition, the sensor properties were improved with the addition of La_2O_3, but the desired improvement could not be achieved with the addition of Fe_2O_3.

References

[1] Yamazoe N, Shimanoe K. New perspectives of gas sensor technology. Sensors and Actuators B: Chemical (2009) 138(1):100–107. doi:10.1016/j.snb.2009.01.023.

[2] Yamazoe N, Shimanoe K. Roles of Shape and Size of Component Crystals in Semiconductor Gas Sensors. Journal of The Electrochemical Society (2008) 155(4):J85-J85. doi:10.1149/1.2832655.

[3] Majumder, S., Hussain, S., Bhar, R., Pal, A.K. Liquid petroleum gas sensor based on SnO2/Pd composite films deposited on Si/SiO2 substrates. Vacuum (2007) 81(8):985–996.

[4] Ehsani M, Hamidon MN, Pah LK. Influence of Pt on structural and morphologycal properties of La2O3 / SnO2 thick film. Research Journal of Chemistry and Environment (2013) 17(10):35–40.

[5] Şahin E. Ekran Baskı Yöntemi Ile Metal Oksit Gaz Sensörü Fabrikasyonu [Metal Oxide Gas Sensor Fabrication With Screen Printing Method]. Master Thesis. Ataturk University. Erzurum (2017).

[6] Martadi S, Sulthoni MA, Wiranto G, Surawijaya A, Herminda ID, editors. Design and Fabrication of PVA-Based Relative Humidity Sensors Using Thick Film Technology (2019).

[7] Guidi V, Butturi MA, Carotta MC, Cavicchi B, Ferroni M, Malagù C, et al. Gas sensing through thick film technology. Sensors and Actuators B: Chemical (2002) 84(1):72–77. doi:10.1016/S0925-4005(01)01077-2.

[8] Ehsani M, Hamidon MN, Toudeshki A, Abadi MHS, Rezaeian S. CO 2 Gas Sensing Properties of Screen-Printed La 2 O 3 /SnO 2 Thick Film. IEEE Sensors Journal (2016) 16(18):6839–6845. doi:10.1109/JSEN.2016.2587779.

[9] Bagal LK, Patil JY, Vaishampayan MV, Mulla IS, Suryavanshi SS. Effect of Pd and Ce on the enhancement of ethanol vapor response of SnO2 thick films. Sensors and Actuators B: Chemical (2015) 207:383–390. doi:10.1016/j.snb.2014.10.021.

[10] Chachuli S, Hamidon MN, Mamat M, Ertugrul M, Abdullah N. A Hydrogen Gas Sensor Based on TiO2 Nanoparticles on Alumina Substrate. Sensors (2018) 18(8):2483. doi:10.3390/s18082483.

[11] Abadi MHS, Hamidon MN, Shaari AH, Abdullah N, Misron N, Wagiran R. Characterization of Mixed xWO3(1-x)Y2O3 Nanoparticle Thick Film for Gas Sensing Application. Sensors (2010) 10(5):5074–5089. doi:10.3390/s100505074.

[12] İskenderoğlu D, Güney H. Synthesis and characterization of ZnO:Ni thin films grown by spray-deposition. Ceramics International (2017) 43(18):16593–16599. doi:10.1016/j.ceramint.2017.09.047.

[13] Zhong WW, Liu FM, Cai LG, Zhou CC, Ding P, Zhang H. Annealing effects of co-doping with Al and Sb on structure and optical–electrical properties of the ZnO thin films. Journal of Alloys and Compounds (2010) 499(2):265–268.
[14] Miskovic G, Aleksic O, Nikolic M, Nicolics J, Radosavljevic G, Zorka, et al. Nanostructured SnO2 thick films for gas sensor application: analysis of structural and electronic properties. IOP Conf. Series: Materials Science and Engineering 108.
[15] Vasiljevic Z, Lukovic D, Nikolic M, Tasic N, Mitric M. Nanostructured Fe2O3/TiO2 thick films: Analysis of structural and electronic properties. Ceramics International (2015) 41:6889–6897.
[16] Pugh D, Hailes S, Parkin I. A gas-sensing array produced from screenprinted, zeolite-modified chromium titanate. Meas. Sci. Technol (2015) 26:085102 9.
[17] Chang L, Choi J, Park Y. Development of metal-loaded mixed metal oxides gas sensors for the detection of lethal gases. Journal of Industrial and Engineering Chemistry (2015) 29:321–329.
[18] Vincenzi D, Butturi MA, Stefancich M, Malagu C, Guidi V, Carotta MC, et al. Low-powerthick-film gas sensor obtained by a combination of screen printing and micromachining techniques. Thin Solid Films (2001) 391:288–292.